Published in final edited form as:
J Magn Reson Imaging. 2011 October ; 34(4): 880–886. doi:10.1002/jmri.22670.

MR Elastography of the kidneys: feasibility and reproducibility in young healthy adults

Olivier Rouvière, MD, PhD[1,2], **Rémi Souchon, PhD**[2], **Gaële Pagnoux, MD**[1], **Jean-Michel Ménager, MD**[3], and **Jean-Yves Chapelon, PhD**[2]

[1] Hospices Civils de Lyon, Department of Urinary and Vascular Radiology, Hôpital Edouard Herriot, Lyon, F-69437, France; Université de Lyon, Lyon, F-69003, France; Université Lyon 1, faculté de médecine Lyon Est, Lyon, F-69003, France

[2] Inserm, U556, Lyon, F-69424, France

[3] SCM IRM Lyon-Villeurbanne, Villeurbanne, F-69100, France

Abstract

Purpose—To evaluate the feasibility and reproducibility of renal Magnetic Resonance Elastography (MRE) in young healthy volunteers.

Material and methods—Ten volunteers underwent renal MRE twice at a 4-5 week interval. The vibrations (45 and 76 Hz) were generated by a speaker positioned beneath the volunteers' back and centered on their left kidney. For each frequency, three sagittal slices were acquired (8 phase offsets per cycle, motion-encoding gradients successively positioned along the three directions of space). Shear velocity images were reconstructed using the curl operator combined with the local frequency estimation (LFE) algorithm.

Results—The mean shear velocities measured in the renal parenchyma during the two examinations were not significantly different and exhibited a mean variation of 6% at 45 Hz and 76 Hz. The mean shear velocities in renal parenchyma were 2.21±0.14 m/s at 45 Hz (shear modulus of 4.9±0.5 kPa) and 3.07±0.17 m/s at 76 Hz (9.4±0.8 kPa, $p<0.01$). The mean shear velocities in the renal cortex and medulla were respectively 2.19±0.13 m/s and 2.32±0.16 m/s at 45 Hz ($p=0.002$) and 3.06±0.16 m/s and 3.10±0.22 m/s at 76 Hz ($p=0.13$).

Conclusion—Renal MRE was feasible and reproducible. Two independent measurements of shear velocities in the renal parenchyma of the same subjects showed an average variability of 6%.

Keywords

Elastography; Magnetic Resonance Elastography; Kidney; Fibrosis; Chronic renal failure; Healthy volunteers

Introduction

Many different mechanisms induce glomerular injury, including glomerulonephritis, hypertensive nephrosclerosis and diabetic nephropathy. However, once renal damage reaches a certain threshold, progression of renal disease is consistent, and largely independent of the initial insult. This common pathway to end-stage renal failure is mainly due to tubulointerstitial damage characterized by tubular atrophy, loss of peritubular

Corresponding author: Pr Olivier Rouvière, Department of Urinary and Vascular Radiology, Pavillon P Radio, Hôpital Edouard Herriot, 69437 Lyon Cedex 03 – France. Tel: (+33) 472 11 09 51 / Fax: (+33) 472 11 09 54; olivier.rouviere@netcourrier.com.

capillaries and interstitial fibrosis. Mechanisms leading to kidney failure via tubulointerstitial damage and development of fibrosis are mostly massive proteinuria and chronic hypoxia. Fibrosis further impairs oxygen diffusion and supply to tubular cells, rendering a vicious cycle (1-4).

Thus, in the assessment of chronic renal failure, fibrosis is a major histological feature and may be an important surrogate endpoint for prognosis and monitoring of treatment response. Besides, some investigations suggest that fibrosis might be reversible, at least in the liver, when the cause is treated (5-7), emphasizing the need for an early detection and quantification of this fibrosis.

Currently, the extent of interstitial fibrosis is evaluated by renal biopsy which has several drawbacks: it is a semi-quantitative approach with wide interobserver variability (8, 9), it is prone to sampling errors and associated with significant morbidity (10-12). Thus a non-invasive, truly quantitative method of interstitial fibrosis monitoring would be desirable.

Diffusion-weighted and Blood Oxygenation Level Dependent (BOLD) MRI findings have been shown to be correlated to renal function (13-17), but no data have been published as to their correlation with the degree of fibrosis. Blood or urinary markers of fibrosis are also currently evaluated but none is used in clinical practice yet (18-20).

Several methods can estimate tissue stiffness (and thus, the degree of fibrosis) by measuring the velocity of shear waves traveling through the organ of interest. They have been mostly used in liver. The ultrasound-based transient elastography (Fibroscan™ device) is able to discriminate the different stages of liver fibrosis with a quadratic trend of the curve plotting histologic scores versus elasticity measurements (21-24). Among patients with cirrhosis, stiffness thresholds predicting the onset of specific complications (ascites, oesophageal bleeding, hepatocarcinoma, etc…) have been identified (21). However, this technique is limited by its 1D nature that does not allow the exploration of the entire liver.

Magnetic resonance Elastography (MRE) (25, 26) has also been successfully used to assess liver fibrosis. The shear stiffness of normal liver was found to be approximately 2 kPa by several independent groups, using vibrating frequencies of 50-90 Hz (27-29). As ultrasound-based transient elastography, MRE can discriminate the different stages of liver fibrosis, with the same quadratic trend of the fibrosis/elasticity curve (27, 29, 30). MRE has the advantage of being intrinsically a 2D technique and can be associated to conventional liver imaging at the same time. Thus, MRE has also been used for other applications such as characterizing focal liver lesions (31), and in other organs such as breast, muscle, prostate or brain (32, 33).

The purpose of this study was to evaluate the feasibility and the reproducibility of renal MRE in healthy volunteers. Our specific goals were to: 1) assess the feasibility of the technique using an external driver delivering low-frequency (<100 Hz) vibrations, 2) describe the shear stiffness of normal renal parenchyma obtained at these frequencies, 3) evaluate the repeatability of the measurements by performing, on the same subjects, two MRE examinations separated by a four-week interval.

Material and Methods

Volunteers

Ten healthy volunteers (5 men, 5 women) with no history of personal or familial kidney disease were enrolled in the study. Their mean age, weight, height and body mass index were 26 ± 2 years (24-30 years), 64 ± 12 kg (50-82 kg), 173 ± 8 cm (162-184 cm) and 21 ±

2 (18-24), respectively. All volunteers underwent renal MRE twice. The delay between the two MRE examinations was 33 ± 3 days (28-35 days). As of today, it is unknown if physiological state (hydration) influences the stiffness of the kidney. To maintain uniform physiological state in all the subjects, the volunteers were instructed to have a light meal 2-3 hours before the examination and to stop drinking one hour before.

This study was approved by our Institutional Review Board. All volunteers gave written informed consent after the nature of the study had been explained to them.

MRE acquisitions

All examinations were performed on a 1.5T MR Scanner (General Electric Healthcare, HD Excite). The vibrations were generated by a speaker (Eminence Kappa Pro-15A) mounted in a sealed enclosure and driven by a signal generator (Agilent 33120A) and an amplifier (Behringer EP 2500). The vibrations were applied to the skin of the volunteers using an 8-cm in diameter, 4-cm thick passive driver (a drumlike device) embedded in a foam cushion. A 5-m long, flexible, braid reinforced, PVC hose with a 25-mm inner diameter, served as a vibration waveguide between the speaker and the passive driver. The output power of the amplifier was constant in all experiments. The wave guide induced attenuation of the vibrations, hence the need for a powerful audio amplifier.

The volunteers were installed on the foam cushion, in supine position. The passive driver was positioned in their back, its center corresponding approximately to the center of the left kidney. Two vibration frequencies, among the resonance frequencies of the set-up, were tested (45 and 76Hz). These frequencies were chosen as a trade-off between wave penetration and spatial resolution (see discussion). An external 8-channel phased-array coil was used for signal reception. MRE wave images were collected with a gradient echo-based MRE sequence developed by the MR Research Laboratory of the Mayo Clinic (Dr R.L. Ehman). The image parameters were : TR 52.6-92.1 ms, TE 31-35 ms, flip angle 26°, FOV 48 × 36 cm^2, matrix 256 × 64 (frequency × phase), slice thickness 5 mm, one (45 Hz) or two (76 Hz) cycles of motion encoding gradients (MEG) with an amplitude of 14.1 mT/m. The three components of the displacement vectors were acquired along the three standardized directions: Head-Feet (HF), Antero-Posterior (AP) and Right-Left (RL) in three contiguous sagittal slices passing through the left kidney (our driver was not powerful enough to induce detectable waves in both kidneys). The acquisitions were performed at end-expiration. A total of 8 images (or “phase offsets”) were acquired per vibration cycle. The data were used to verify that displacement was effectively oscillating at the required frequency (Fourier analysis with 8 samples per cycles provided information up to the 4^{th} harmonic). A time delay of 3 s was used between the onset of the vibration and the MR acquisition, to avoid unwanted transient effects.

Assessment of MRE tolerability

After each MRE examination, the volunteers scored four tolerance items (length of examination, position in the magnet, repetitions of breath-holds, vibrations) by using, for each of them, the same 5-point scale (1: very bearable; 2: bearable; 3: unpleasant; 4: very unpleasant; 5: unbearable)

Wave inversion

The curl operator removes the compression wave at the cost of increased noise in the wave images. Sinkus et al. initially proposed to combine it with a direct inversion algorithm (34). However this combination is highly sensitive to noise because it involves three consecutive gradient operations on the wave images. In our study, we chose to combine the curl operator with the LFE algorithm, known for its robustness to noise.

The phase images were first unwrapped with a dedicated software (MRE-LAB, Mayo Clinic), using a minimum discontinuity algorithm. The unwrapped phase images were then converted to displacement images by multiplication by a scaling factor, as described elsewhere (25).

A selective 7×7 median filter with a 1.2 μm threshold, a standard 3×3 median filter, a 3×3 moving average filter, and a frequency-selective FFT filter (35), were consecutively applied to smooth the displacement images. Then, the curl operator was applied to remove the contribution of the longitudinal waves (34). The curl operator takes 2 components of the displacement vector and combines them into a single value. Hence three combinations exist, respectively denoted APxRL, RLxHF and HFxAP. Each combination provides a new « wave movie » that obeys the same equation of propagation as the displacement (34), and can be analyzed independently to estimate the shear velocity.

Next, the images were processed in MRE-LAB with a 4^{th} order Butterworth directional filter (36) designed to preserve the propagation in the posterior to anterior direction. The cutoff frequencies in k-space corresponded to 1-12 cm wavelength at 45 Hz, and to 0.6-12 cm wavelength at 76 Hz.

Finally, the images were processed in MRE-LAB with a 2D local frequency estimator (LFE) to determine the local wavelength λ. The local shear velocity $c = f\lambda$ was estimated from the wavelength.

The same process was applied independently to each combination (APxRL, RLxHF and HFxAP), providing 3 shear velocity images. The results measured on the 3 images were averaged, except in Table 3 where individual measurements are reported.

We investigated the influence of the processing options by (1) disabling only the directional filter (all other parameters unchanged), (2) disabling only the curl operator.

Vibration amplitude and shear velocity

Regions of Interest (ROIs) encompassing the renal parenchyma and excluding perirenal tissues and the renal sinus were positioned on magnitude images. Then, ROIs encompassing only the renal cortex and only the renal medulla were positioned on magnitude images. All these ROIS were then reported on the phase images and the mean displacement and shear velocity within these ROIs were calculated.

Reproducibility

The variability between the mean shear velocities V1 and V2 measured during MRE 1 and 2, was expressed as a percentage and calculated according to the following formula: $\text{variability}=(|V1 - V2|)/((V1+V2)/2)$.

Statistical Analysis

Comparisons of mean shear velocities were performed using the non-parametric Wilcoxon Matched-Pairs Signed-Ranks Test. A p value <0.05 was considered significant. Bland-Altman plots comparing the results of the two MRE examinations on the same volunteers were also obtained.

Results

Duration and tolerance of MRE examinations

No technical failure was encountered and MRE was successfully performed in all volunteers. The mean duration of the MRE examinations (including the time needed to position the driver in front of the kidney) was 75 ± 13 minutes (56-105 minutes). Figure 1 shows the results of the tolerance questionnaires of the 20 MRE examinations. All items received tolerance scores of 1 (very bearable) or 2 (bearable), the only exception being one score 3 (unpleasant) for the duration of the first examination, which was the longest one (105 minutes) because of the time needed for the initial setup.

Vibration amplitude in renal parenchyma

The mean vibration amplitude (averaged over all MRE examinations, *N*=20) ranged from 8 μm up to 35 μm in renal parenchyma (Table 1). It was approximately twice as large at 45 Hz as at 76 Hz. The vibration amplitude in the RL direction was approximately half the vibration amplitude in the other directions.

Reproducibility

Figure 2 illustrates typical shear velocity images at 45 Hz and 76 Hz. Table 2 shows the shear velocities measured in the renal parenchyma at 45 Hz and 76 Hz, for the two MRE examinations. There was no significant difference between the mean shear velocity measured during the first and the second MRE examination, both at 45 Hz (2.25 ± 0.14 vs. 2.18 ± 0.13 m/s; p=0.23) and 76 Hz (3.04 ± 0.19 vs. 3.10 ± 0.16 m/s; p=0.32). The mean variation between the two measurements was 6% (2-16%) at 45 Hz and 6% (1-14%) at 76 Hz. The good reproducibility of the MRE examination is visible in the Bland-Altman plots (Figures 3 and 4).

Shear velocity in renal parenchyma

When the values obtained at MRE 1 and 2 were averaged, the overall mean shear velocity was 2.21 ± 0.14 m/s at 45 Hz (corresponding to a shear modulus of 4.9 ± 0.5 kPa) and 3.07 ± 0.17 m/s at 76 Hz (shear modulus of 9.4 ± 0.8 kPa). The overall mean shear velocities measured at 45 Hz and 76 Hz were significantly different ($p<0.01$).

Shear velocity in cortex and medulla

The mean shear velocities (average of values obtained at MRE 1 and 2) in the renal cortex and medulla were respectively 2.19 ± 0.13 m/s and 2.32 ± 0.16 m/s at 45 Hz (p=0.002) and 3.06 ± 0.16 m/s and 3.10 ± 0.22 m/s at 76 Hz (p=0.13).

Influence of processing options—The results are summarized in Table 3. The method we chose provided consistent measurements for all components. Disabling the directional filter did not significantly modify the elasticity images obtained with the HFxAP component of the curl vector. However, the shear velocities obtained from the two other components were higher. Disabling the curl operator also resulted in increased shear velocities measurements. The images obtained from the AP component of the displacement (i.e. in the main direction of compression by the driver membrane) were most affected.

Discussion

Our study showed renal MRE using an external driver was feasible in humans. Renal shear stiffness measurements were possible in all volunteers at both frequencies, with shear stiffness of 4.9 ± 0.5 kPa at 45 Hz and 9.4 ± 0.8 kPa at 76 Hz. These data are close to those

reported by Venkatesh et al. (37) in a preliminary study in five healthy volunteers (7.3 ± 1.7 kPa at 90 Hz). Two recent studies with ultrasonic transient elastography (Siemens Virtual Touch™) reported shear velocities very close to our measurements: 2.24 m/s in renal cortex in healthy volunteers (38), and shear velocities in the 2.1 – 3.3 m/s range for kidney transplants with BANFF score 0 (39). However the comparison with these results is difficult because the central frequency of the transient push (or equivalently the push duration) was not specified.

A recent study evaluated the use of the Fibroscan™ device in renal transplants (40). The authors reported a Young's modulus of 32.7 ± 14.9 kPa in the parenchyma. This result corresponds to a shear velocity of 3.3 m/s at 50 Hz (central frequency of the Fibroscan). However, because this is a 1D technique, the measurements were performed blindly. As a consequence, the region where the measurements were made may have included peri-renal/sinusal tissues.

The duration of our imaging protocol is not compatible with clinical practice. However MRE exams can be performed with only 2 images per cycle instead of 8, resulting in a 4-fold reduction in acquisition time. Additionally, echo planar imaging (EPI)-based MRE is becoming available, as well as simultaneous multi-frequency MRE systems (41), allowing further reduction in acquisition time.

The significant difference between the renal stiffness measured at 45 Hz and 76 Hz conveys that renal parenchyma is visco-elastic rather than purely elastic. It is now well known that the MRE-measured shear modulus of soft tissue is dependent on the frequency of applied mechanical waves (42-44). That is why the term ‘shear stiffness’ is often used to describe the shear modulus at a specific frequency. However, it should be fully understood that the formula that calculates the shear modulus from the measured velocity of the waves ($\mu = \rho c^2$) is valid only in purely elastic tissues. In addition, estimating shear stiffness from shear velocity becomes challenging whenever the wavelength of the vibration is of the same order as the dimension of the organ (45), as was the case in our study (wavelength ~50 mm at 45 Hz, and ~40 mm at 76 Hz). Therefore, we chose to report wave velocities (that are physically measurable values) instead of shear modulus values (the calculation of which are based on unverifiable assumptions). An alternative to reporting shear velocities would be reporting the corresponding complex (dynamic) modulus. However this approach requires the use of a direct inversion algorithm and is beyond the scope of the present study.

Our method provided consistent shear velocity measurements for all encoding directions (Table 3). Disabling the directional filter did not significantly modify the elasticity images obtained with the HFxAP component of the curl vector. However, the shear velocities obtained from the two other components were higher. These discrepancies might be explained by two reasons: first, for the HFxRL and APxRL combinations, the curl operation involved a spatial gradient in the slice direction, where sampling was poor because of slice thickness; second, the RL component of the displacement was the lowest of the three displacement components (i.e. poor phase SNR), probably because the images were obtained near the centre of the driver where this component is minimal (26).

With the curl operator disabled, the shear velocities were higher, especially with the AP component of the displacement. This observation suggests that compression waves induced an overestimation of the shear velocity measurements.

Whether MRE will be able to disclose maps of elasticity showing the spatial distribution of fibrosis in kidneys is beyond the scope of this feasibility study. Indeed, the ability of the technique to resolve two structures of different stiffness depends on the stiffness contrast, on the relative size of the structures as compared to the spatial resolution of the elasticity maps

(shear waves' half-wavelength (46)), and on the amplitude of the shear waves (noise of the measurements). In our study, the shear waves' half-wavelength was 25 mm at 45 Hz, and 20 mm at 76 Hz. It was therefore a major limiting factor.

Better spatial resolution could be obtained by using other wave inversion algorithms (34) and/or higher vibration frequencies. We did not use frequencies higher than 76 Hz because preliminary experiments showed that our driving system induced insufficient displacements at higher frequencies. In the future, more powerful vibrating external setups can be used, and/or alternate methods, such as the use of ultrasound radiation force, can be developed. It has indeed been shown that the ultrasound radiation force can generate shear waves directly inside the tissue of interest, avoiding the resolution/penetration tradeoff (47). Transient MRE images of porcine kidneys have been obtained ex vivo by delivering high frequency shear waves directly into the renal cortex (48). However, because of substantial heat deposition at the ultrasonic focal point (+ 6°C for the acquisition of a single MRE image ex vivo using a conventional gradient-echo based MRE sequence (49)), this technique cannot be used in humans for the moment.

We obtained higher shear wave velocities in the medulla than in the cortex at both frequencies. This observation was consistent with the images presented by Shah et al (50) in rat kidney, and with preliminary results obtained with transient MR elastography in porcine kidney (48). However, the difference was small (2.19 m/s vs. 2.32 m/s) and only significant at 45 Hz. These results should be taken with care given the poor spatial resolution of the images compared to the thickness of the cortex (typ. ~ 10 mm).

In conclusion, this feasibility study showed that MRE of native kidneys in young adults was feasible, with a mean shear velocity of 2.21±0.14 m/s at 45 Hz (shear modulus of 4.9±0.5 kPa) and 3.07±0.17 m/s at 76 Hz (9.4±0.8 kPa) in the renal parenchyma. The technique was reproducible, with a 6% mean intra-volunteer variability of the measurements. These good results should foster further research to evaluate the accuracy of MRE in non-invasively assessing the degree of fibrosis in native kidneys and renal transplants.

Acknowledgments

The authors are deeply thankful to Richard L Ehman and Roger C Grimm for providing the MRE sequence and the MRE-LAB software, and to Richard L Ehman and Meng Yin for their comments on the manuscript. They also thank Dr Pierre-Jean Ternamian and the technologists of SCM IRM Lyon-Villeurbanne for their precious help.

Funding information: This work was supported by Hospices Civils de Lyon (Actions incitatives 2007), by NIH grant EB001981, and by SCM IRM Lyon Villeurbanne.

References

1. Bohle A, Mackensen-Haen S, von Gise H. Significance of tubulointerstitial changes in the renal cortex for the excretory function and concentration ability of the kidney: a morphometric contribution. Am J Nephrol. 1987; 7:421–433. [PubMed: 3439552]
2. Nakagawa T, Kang DH, Ohashi R, et al. Tubulointerstitial disease: role of ischemia and microvascular disease. Curr Opin Nephrol Hypertens. 2003; 12:233–241. [PubMed: 12698060]
3. Nangaku M. Mechanisms of tubulointerstitial injury in the kidney: final common pathways to end-stage renal failure. Intern Med. 2004; 43:9–17. [PubMed: 14964574]
4. Nath KA. Tubulointerstitial changes as a major determinant in the progression of renal damage. Am J Kidney Dis. 1992; 20:1–17. [PubMed: 1621674]
5. Dufour JF, DeLellis R, Kaplan MM. Reversibility of hepatic fibrosis in autoimmune hepatitis. Ann Intern Med. 1997; 127:981–985. [PubMed: 9412303]

6. Shiratori Y, Imazeki F, Moriyama M, et al. Histologic improvement of fibrosis in patients with hepatitis C who have sustained response to interferon therapy. Ann Intern Med. 2000; 132:517–524. [PubMed: 10744587]
7. Nelson DR, Lauwers GY, Lau JY, Davis GL. Interleukin 10 treatment reduces fibrosis in patients with chronic hepatitis C: a pilot trial of interferon nonresponders. Gastroenterology. 2000; 118:655–660. [PubMed: 10734016]
8. Seron D, Moreso F, Fulladosa X, Hueso M, Carrera M, Grinyo JM. Reliability of chronic allograft nephropathy diagnosis in sequential protocol biopsies. Kidney Int. 2002; 61:727–733. [PubMed: 11849416]
9. Furness PN, Taub N. International variation in the interpretation of renal transplant biopsies: report of the CERTPAP Project. Kidney Int. 2001; 60:1998–2012. [PubMed: 11703620]
10. Eiro M, Katoh T, Watanabe T. Risk factors for bleeding complications in percutaneous renal biopsy. Clin Exp Nephrol. 2005; 9:40–45. [PubMed: 15830272]
11. Furness PN, Philpott CM, Chorbadjian MT, et al. Protocol biopsy of the stable renal transplant: a multicenter study of methods and complication rates. Transplantation. 2003; 76:969–973. [PubMed: 14508363]
12. Preda A, Van Dijk LC, Van Oostaijen JA, Pattynama PM. Complication rate and diagnostic yield of 515 consecutive ultrasound-guided biopsies of renal allografts and native kidneys using a 14-gauge Biopty gun. Eur Radiol. 2003; 13:527–530. [PubMed: 12594555]
13. Juillard L, Lerman LO, Kruger DG, et al. Blood oxygen level-dependent measurement of acute intra-renal ischemia. Kidney Int. 2004; 65:944–950. [PubMed: 14871414]
14. Namimoto T, Yamashita Y, Mitsuzaki K, Nakayama Y, Tang Y, Takahashi M. Measurement of the apparent diffusion coefficient in diffuse renal disease by diffusion-weighted echo-planar MR imaging. J Magn Reson Imaging. 1999; 9:832–837. [PubMed: 10373031]
15. Thoeny HC, De Keyzer F, Oyen RH, Peeters RR. Diffusion-weighted MR imaging of kidneys in healthy volunteers and patients with parenchymal diseases: initial experience. Radiology. 2005; 235:911–917. [PubMed: 15845792]
16. Thoeny HC, Zumstein D, Simon-Zoula S, et al. Functional evaluation of transplanted kidneys with diffusion-weighted and BOLD MR imaging: initial experience. Radiology. 2006; 241:812–821. [PubMed: 17114628]
17. Xu Y, Wang X, Jiang X. Relationship between the renal apparent diffusion coefficient and glomerular filtration rate: preliminary experience. J Magn Reson Imaging. 2007; 26:678–681. [PubMed: 17729335]
18. Wu I, Parikh CR. Screening for kidney diseases: older measures versus novel biomarkers. Clin J Am Soc Nephrol. 2008; 3:1895–1901. [PubMed: 18922990]
19. Ghoul BE, Squalli T, Servais A, et al. Urinary procollagen III aminoterminal propeptide (PIIINP): a fibrotest for the nephrologist. Clin J Am Soc Nephrol. 2010; 5:205–210. [PubMed: 20089486]
20. Boratynska M. Urine excretion of transforming growth factor-beta1 in chronic allograft nephropathy. Ann Transplant. 1999; 4:23–28. [PubMed: 10850587]
21. Foucher J, Chanteloup E, Vergniol J, et al. Diagnosis of cirrhosis by transient elastography (FibroScan): a prospective study. Gut. 2006; 55:403–408. [PubMed: 16020491]
22. Fraquelli M, Rigamonti C, Casazza G, et al. Reproducibility of transient elastography in the evaluation of liver fibrosis in patients with chronic liver disease. Gut. 2007; 56:968–973. [PubMed: 17255218]
23. Boursier J, Vergniol J, Sawadogo A, et al. The combination of a blood test and Fibroscan improves the non-invasive diagnosis of liver fibrosis. Liver Int. 2009; 29:1507–1515. [PubMed: 19725892]
24. Sandrin L, Fourquet B, Hasquenoph JM, et al. Transient elastography: a new noninvasive method for assessment of hepatic fibrosis. Ultrasound Med Biol. 2003; 29:1705–1713. [PubMed: 14698338]
25. Muthupillai R, Lomas DJ, Rossman PJ, Greenleaf JF, Manduca A, Ehman RL. Magnetic resonance elastography by direct visualization of propagating acoustic strain waves. Science. 1995; 269:1854–1857. [PubMed: 7569924]

26. Yin M, Rouviere O, Glaser KJ, Ehman RL. Diffraction-biased shear wave fields generated with longitudinal magnetic resonance elastography drivers. Magn Reson Imaging. 2008; 26:770–780. [PubMed: 18467059]
27. Huwart L, Peeters F, Sinkus R, et al. Liver fibrosis: non-invasive assessment with MR elastography. NMR Biomed. 2006; 19:173–179. [PubMed: 16521091]
28. Klatt D, Asbach P, Rump J, et al. In vivo determination of hepatic stiffness using steady-state free precession magnetic resonance elastography. Invest Radiol. 2006; 41:841–848. [PubMed: 17099421]
29. Rouviere O, Yin M, Dresner MA, et al. MR elastography of the liver: preliminary results. Radiology. 2006; 240:440–448. [PubMed: 16864671]
30. Huwart L, Sempoux C, Vicaut E, et al. Magnetic resonance elastography for the noninvasive staging of liver fibrosis. Gastroenterology. 2008; 135:32–40. [PubMed: 18471441]
31. Venkatesh SK, Yin M, Glockner JF, et al. MR elastography of liver tumors: preliminary results. AJR Am J Roentgenol. 2008; 190:1534–1540. [PubMed: 18492904]
32. Kemper J, Sinkus R, Lorenzen J, Nolte-Ernsting C, Stork A, Adam G. MR elastography of the prostate: initial in-vivo application. Rofo. 2004; 176:1094–1099. [PubMed: 15346284]
33. Mariappan YK, Glaser KJ, Ehman RL. Magnetic resonance elastography: a review. Clin Anat. 2010; 23:497–511. [PubMed: 20544947]
34. Sinkus R, Tanter M, Xydeas T, Catheline S, Bercoff J, Fink M. Viscoelastic shear properties of in vivo breast lesions measured by MR elastography. Magn Reson Imaging. 2005; 23:159–165. [PubMed: 15833607]
35. Sinkus R, Lorenzen J, Schrader D, Lorenzen M, Dargatz M, Holz D. High-resolution tensor MR elastography for breast tumour detection. Phys Med Biol. 2000; 45:1649–1664. [PubMed: 10870716]
36. Manduca A, Lake DS, Kruse SA, Ehman RL. Spatio-temporal directional filtering for improved inversion of MR elastography images. Med Image Anal. 2003; 7:465–473. [PubMed: 14561551]
37. Venkatesh SK, Yin M, Grimm RC, et al. MR Elastography of the Kidneys: Preliminary Results. Proc Intl Soc Mag Reson Med. 2008; 16:461.
38. Gallotti A, D'Onofrio M, Pozzi Mucelli R. Acoustic Radiation Force Impulse (ARFI) technique in ultrasound with Virtual Touch tissue quantification of the upper abdomen. Radiol Med. 2010; 115:889–897. [PubMed: 20082227]
39. Stock KF, Klein BS, Vo Cong MT, et al. ARFI-based tissue elasticity quantification in comparison to histology for the diagnosis of renal transplant fibrosis. Clin Hemorheol Microcirc. 2010; 46:139–148. [PubMed: 21135489]
40. Arndt R, Schmidt S, Loddenkemper C, et al. Noninvasive evaluation of renal allograft fibrosis by transient elastography--a pilot study. Transpl Int. 2010; 23:871–877. [PubMed: 20158692]
41. Klatt D, Hamhaber U, Asbach P, Braun J, Sack I. Noninvasive assessment of the rheological behavior of human organs using multifrequency MR elastography: a study of brain and liver viscoelasticity. Phys Med Biol. 2007; 52:7281–7294. [PubMed: 18065839]
42. Krouskop TA, Wheeler TM, Kallel F, Garra BS, Hall T. Elastic moduli of breast and prostate tissues under compression. Ultrason Imaging. 1998; 20:260–274. [PubMed: 10197347]
43. Kruse SA, Smith JA, Lawrence AJ, et al. Tissue characterization using magnetic resonance elastography: preliminary results. Phys Med Biol. 2000; 45:1579–1590. [PubMed: 10870712]
44. Zhang M, Nigwekar P, Castaneda B, et al. Quantitative characterization of viscoelastic properties of human prostate correlated with histology. Ultrasound Med Biol. 2008; 34:1033–1042. [PubMed: 18258350]
45. Kolipaka A, McGee KP, Manduca A, et al. Magnetic resonance elastography: Inversions in bounded media. Magn Reson Med. 2009; 62:1533–1542. [PubMed: 19780146]
46. Manduca, A.; Muthupillai, R.; Rossman, PJ.; Greenleaf, JF.; Ehman, RL. Proceedings of the SPIE Medical Imaging, The international Society for Optics and Photonics. Vol. 616. Newport Beach: 1996. Image processing for magnetic resonance elastography.
47. Wu T, Felmlee JP, Greenleaf JF, Riederer SJ, Ehman RL. MR imaging of shear waves generated by focused ultrasound. Magn Reson Med. 2000; 43:111–115. [PubMed: 10642737]

48. Souchon R, Salomir R, Chapelon JY, Beuf O, Rouviere O. Transient Magnetic Resonance Elastography. IRBM. 2009; 30:168–170.

49. Souchon R, Salomir R, Beuf O, et al. Transient MR elastography (t-MRE) using ultrasound radiation force: theory, safety, and initial experiments in vitro. Magn Reson Med. 2008; 60:871–881. [PubMed: 18816871]

50. Shah NS, Kruse SA, Lager DJ, et al. Evaluation of renal parenchymal disease in a rat model with magnetic resonance elastography. Magn Reson Med. 2004; 52:56–64. [PubMed: 15236367]

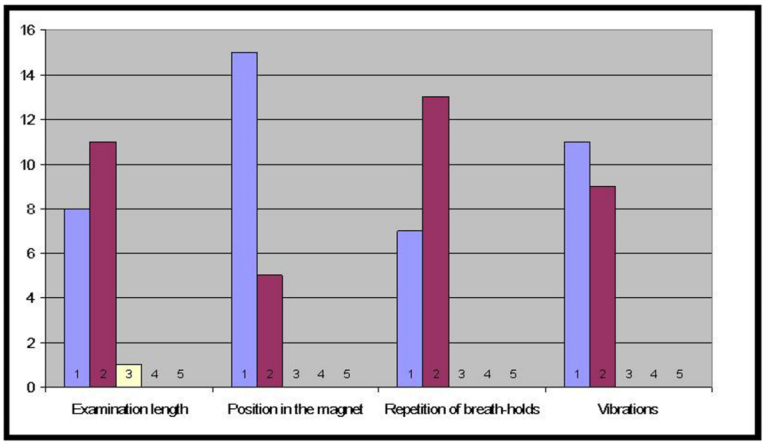

Fig 1.

Results of the tolerance questionnaires of the 20 MRE examinations.

Each item was scored by using the same 5-point scale (1: very bearable; 2: bearable; 3: unpleasant; 4: very unpleasant; 5: unbearable)

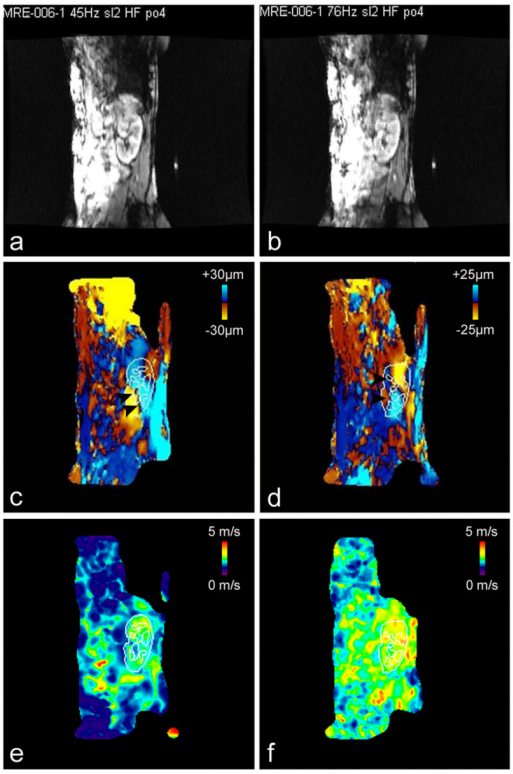

Fig 2.

Images obtained in volunteer 6 (first examination)

2a-b: magnitudes images of the 45 Hz (Fig 2a) and 76 Hz (Fig 2b) MRE acquisitions, showing the position of the kidney

2c-d: corresponding phase images (motion encoding gradients in the Head-Feet direction) obtained at 45 Hz (Fig 2c) and 76 Hz (Fig 2d) and showing shear waves (black arrowheads) traveling through the kidney. The outline (reported from the magnitude images) shows renal cortex and medulla. Such outlines were used to calculate the mean velocities in the cortex, the medulla and the whole parenchyma (cortex and medulla).

2e-f: corresponding shear velocity maps (HFxAP combination) obtained at 45 Hz (Fig 2e) and 76 Hz (Fig 2f).

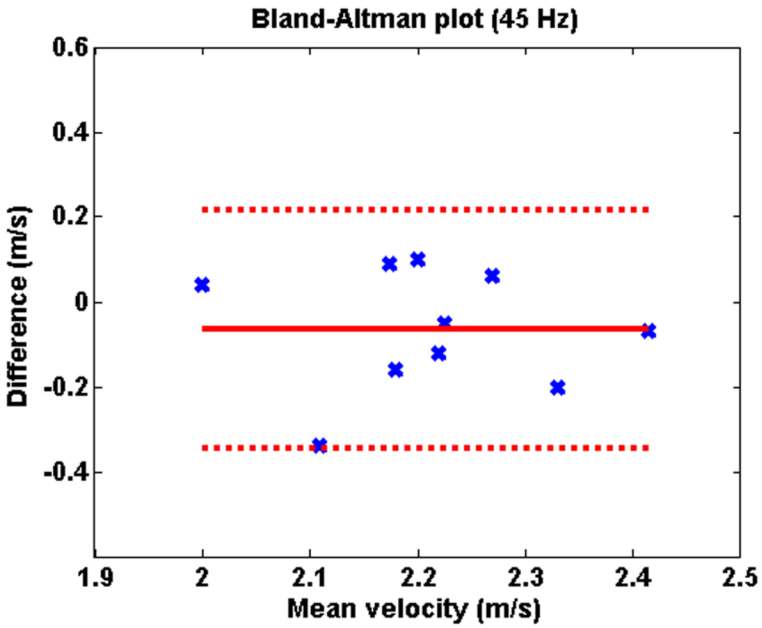

Fig 3.

Bland-Altman plot showing the reproducibility of the measurements of shear waves velocities in the renal parenchyma at MRE 1 and 2 at 45 Hz

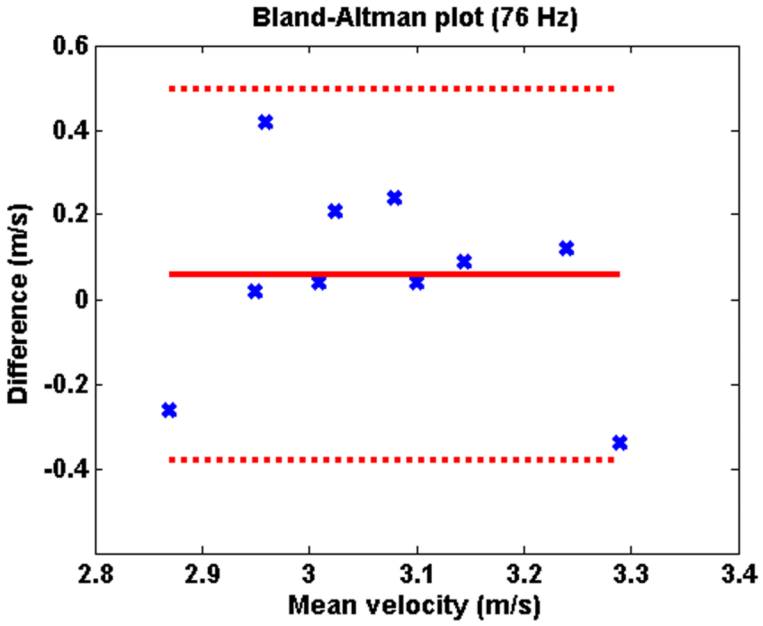

Fig 4.

Bland-Altman plot showing the reproducibility of the measurements of shear waves velocities in the renal parenchyma at MRE 1 and 2 at 76 Hz

Table 1

Vibration amplitude (mean ± standard deviation) in the renal parenchyma as a function of the vibrating frequency and the direction of the motion encoding gradients (in microns)

	HF	AP	RL
45 Hz	33 ± 10	35 ± 9	19 ± 7
76 Hz	16 ± 5	18 ± 4	8 ± 2

HF: motion encoding gradients in the Head-Feet direction.
AP: motion encoding gradients in the Antero-Posterior direction.
RL: motion encoding gradients in the Right-Left direction.

Table 2

Shear velocities measured in the renal parenchyma at 45 Hz and 76 Hz during the two MRE examinations

Volunteers	45 HZ			76 HZ		
	MRE 1	MRE 2	Mean	MRE 1	MRE 2	Mean
1	2.26	2.10	2.18	2.99	3.03	3.01
2	2.13	2.22	2.18	3.00	2.74	2.87
3	2.24	2.30	2.27	2.96	3.20	3.08
4	1.98	2.02	2.00	2.94	2.96	2.95
5	2.15	2.25	2.20	2.75	3.17	2.96
6	2.28	2.16	2.22	3.08	3.12	3.10
7	2.43	2.23	2.33	3.18	3.30	3.24
8	2.28	1.94	2.11	2.92	3.13	3.02
9	2.25	2.20	2.23	3.10	3.19	3.15
10	2.45	2.38	2.42	3.46	3.12	3.29
Mean	2.25 ± 0.14	2.18 ± 0.13	2.21 ± 0.14	3.04 ± 0.19	3.10 ± 0.16	3.07 ± 0.17

Shear velocities are expressed in m/s.

Table 3

Influence of processing options on shear velocity measurements.

Frequency	Method	Component		
		APxRL	RLxHF	HFxAP
45 Hz	Curl + DF	2.3 ± 0.3	2.2 ± 0.3	2.3 ± 0.2
	No DF	2.7 ± 0.3	2.8 ± 0.5	2.3 ± 0.2
		HF (phase)	AP (freq)	RL (slice)
	No Curl	2.6 ± 0.2	3.2 ± 0.3	2.5 ± 0.4
		APxRL	RLxHF	HFxAP
76 Hz	Curl + DF	3.2 ± 0.4	3.1 ± 0.3	3 ± 0.3
	No DF	4 ± 0.5	3.8 ± 0.6	3.2 ± 0.2
		HF (phase)	AP (freq)	RL (slice)
	No Curl	3.4 ± 0.3	4.3 ± 0.4	3.2 ± 0.4

Velocities are reported as mean ± standard deviation, in m/s. The method we chose (*Curl + DF*) provided consistent measurements for all components. Disabling the directional filter (*No DF*) had no significant influence of the velocities measured from the HFxAP component. Disabling the curl operator (*No Curl*) resulted in increased velocity measurements, especially for displacement in the AP direction.